

Article

Simulation Analysis of Skew Collision of Needle Roller Bearing Used in Precision Cycloid Reducer

Yue Sun, Ying-Hui Zhang * and Wei-Dong He

School of Mechanical Engineering, Dalian Jiaotong University, Dalian 116028, China

* Correspondence: zyh@djtu.edu.cn

Abstract: In order to improve the service life of the needle roller bearing used in a precision cycloid reducer, and to reveal the skew and collision phenomenon of the needle roller bearing, based on the force analysis of the transmission mechanism of the cycloid reducer and considering the friction between the cycloid wheel, needle roller, cage, and crank shaft, the dynamic contact between the rolling bodies is simulated by the Hertz elastic contact, where the contact between the cage pocket hole and needle roller is equivalent to the spring and damping, and a nonlinear dynamic model of the needle roller bearing is established. The influence of different load and cage clearances on the deflection impact of the rotating needle roller bearing is calculated. The results show that the inclination of rollers is different under different pocket clearances, and the larger the pocket gap, the greater the fluctuation of the roller inclination angle; the action force of the crank shaft on the roller suppresses the deflection of the roller; the impact force of the roller on the cage has periodicity, which is consistent with the impact force of the crank shaft on the roller. The impact force of the cage is different under different loads, and the greater the load, the more rollers there are in the bearing area, the larger the impact force is, and the smaller the impact force of the rollers in the middle of the bearing zone is, compared with that of the rollers on the two sides; when the load is small, a pocket cage gap of 0.3 mm is selected, and when the load is heavy, a pocket cage gap of 0.2 mm is selected in order to make the bearing run more smoothly.

Keywords: needle roller bearing; pocket clearance; collision and impact; cage; skew



Citation: Sun, Y.; Zhang, Y.-H.; He, W.-D. Simulation Analysis of Skew Collision of Needle Roller Bearing Used in Precision Cycloid Reducer. *Machines* **2023**, *11*, 419. <https://doi.org/10.3390/machines11040419>

Academic Editor: Davide Astolfi

Received: 13 February 2023

Revised: 14 March 2023

Accepted: 23 March 2023

Published: 24 March 2023



Copyright: © 2023 by the authors. Licensee MDPI, Basel, Switzerland. This article is an open access article distributed under the terms and conditions of the Creative Commons Attribution (CC BY) license (<https://creativecommons.org/licenses/by/4.0/>).

1. Introduction

The industrial robot precision cycloid reducer also known as the RV reducer (rotate vector reducer) is a kind of power transmission mechanism that is composed of the front stage of a planetary gear reducer and the rear stage of a cycloid pinwheel reducer. This structure reducer has the characteristics of a large transmission ratio, high precision, small air return, large bearing capacity, high efficiency, low noise, large stiffness, and small return difference, among others.

It is widely used in industrial manipulators and plays the role of a joint bearing. In an RV reducer, as is shown in Figure 1, the arm bearing is a needle roller bearing without inner and outer rings, which is the weak link of the whole reducer; the service life of the whole reducer is determined by its service life. The needle roller bearing is in contact with the crank shaft and the cycloid piece, respectively, and plays a role in transferring power between them. Due to the complex contact load of the rotating needle roller bearing, fatigue failures and a lack of strength easily occur, leading to the short working life of the bearing, which directly affects the working performance of the cycloid reducer.

Therefore, based on the dynamic simulation analysis of the reducer, finding out the law of the oblique collision between the needle roller and the cage under various working conditions, solving the matching problem between different needle roller bearings and different working conditions, and improving the bearing life and performance of precision cycloid reducers are of great significance.

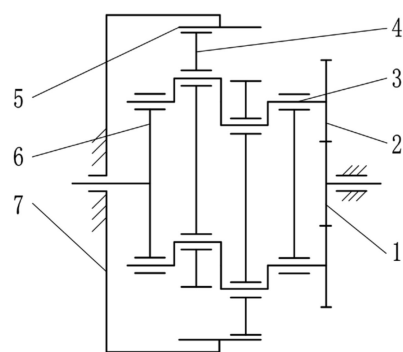


Figure 1. RV 110E gear train transmission diagram: 1—solar wheel; 2—planetary gear; 3—crank shaft; 4—cycloid wheel; 5—pinwheel; 6—planetary rack; 7—pin tooth housing.

Bearings have always been a hot topic for researchers. In recent years, most scholars have mainly focused on rolling bearings. Boesiger et al. obtained the dynamic characteristics and stress of a cage by studying the cage bending deformation and the deformation of the contact area between the roller and the cage [1]; Creju et al. considered the centrifugal forces and roller gyro torques to be solved using the vector method. Based on the written roller and cage differential equation, a complete dynamic analysis of tapered roller bearings was obtained [2]; Meeks and Tran established a non-completely elastic contact model for angular contact ball bearings, which can simulate the six degrees of freedom of rollers and the cage [3]; the incomplete elastic collision in the literature is a kind of collision with damping and kinetic energy loss. Based on the improvement of Persson's contact model, Ciavarella and Decuzzi put forward another small-gap contact impact force model that is suitable for cases involving a very small contact radius and a big enough contact half angle [4].

In recent years, more and more scholars in China have studied the effects of roller collision cages. It was initiated by Cui, who explained the cause of the roller askew and described in detail the effect of the roller askew on the life of a bearing without a cage [5]. The domestic methods for studying the problems related to bearing cages are mainly divided into two categories; one is to use simulation software to analyze all kinds of bearings, but the main research contents are biased towards the stability of the cage. Additionally, because ANSYS, ADAMS, and other software are mainly used for simulation, the collision and friction between the rolling body and the cage cannot be well described.

Pang et al. optimized the pocket hole and inner diameter of a certain type of tank needle roller bearing, reduced the stress of the cage, and verified the rationality of the optimization based on finite element analysis [6]. Based on ANSYS/LS-DYNA, Cui et al. studied the influence of radial clearance and pocket clearance on the dynamic characteristics of the cage, including the cage flexibility and stress distribution [7]. Based on ADAMS simulation of the actual working conditions of the main bearing in a wind farm, Zhang et al. obtained the interaction force between the roller, the inner and outer rings, and the cage, which showed that the roller–cage interaction force is at its maximum when braking [8]. Tu et al. simulated the influence of radial force, axial force, and angular acceleration on ball–cage collisions during deceleration based on ADAMS simulation [9]. Gong et al. established a dynamic simulation model of a flexible cage with a cylindrical roller bearing based on ADAMS simulation, and the dynamic characteristics of bearings under different rotating speeds and loads were analyzed [10].

The other method involves calculating the force between the roller and cage based on various numerical analysis methods. However, the main research contents of most scholars are the relevant factors affecting the collision force of the cage, even if the deflection of the roller is taken into account, but the specific deflection angle of the roller and the position and pose change of the roller cannot be obtained.

Liu et al. defined the occurrence conditions of the collision contact between the rolling body and the cage using fuzzy collision theory and established a dynamic model of the cage to explore the influence of the cage pocket clearance and guide clearance

of the collision force between the cage and rolling body on the stability of the bearing motion [11]. An impact vibration model of the static roller and cage was established by Wang et al., and the variation of cage impact load under different deflection angles, rotating speeds, and static loads was studied [12]. By using the precise integration method and the Adams–Bashforth–Moulton method, the dynamic response of a bearing cage under different guiding modes was studied by Deng et al. [13]. However, it was only proven that an excessive cage clearance ratio was not conducive to the stable operation of a cage. Yao established a single-cage roller with a two-degree-of-freedom collision system and used the fixed-step fourth-order Runge–Kutta method to solve the calculation. This showed that the influence of the impact force on the cage motion was much higher than that of other circumferential forces [14]. However, the system could not describe the actual complex motion characteristics of the bearing well.

Based on a numerical analysis, Ma et al. demonstrated that roller busbar modification can reduce the large contact stress phenomenon at the end of rollers caused by roller deflection and improve the fatigue life of bearings to a certain extent [15]. Zhao et al. analyzed the cause of roller skew and put forward corresponding improvement measures [16]. The critical values of the tapered roller bearing inclination angle with a friction coefficient and cage clearance were obtained by Zhang et al. using the slice method and the fourth-order Runge–Kutta method [17]. Tu et al. established a coupling dynamic model of a rolling bearing and conducted a dynamic analysis of the roller–cage collision with deep groove ball bearings under different working conditions. The results showed that the collision is most severe under rectangular fluctuation conditions [18]. Wang et al. proposed an improved contact–collision model based on the variable recovery coefficient. However, the model only considers the strength and initial collision velocity of the material [19]. Considering the dynamic contact relationship between the roller and ferrule raceway, roller and cage, and cage and guide surface of the ferrule, Wang et al. established a dynamic differential equation of needle roller bearings under revolution and rotation conditions and solved it using the GSTIFF variable step-size integral algorithm; furthermore, the effect of bearing working conditions on cage stress was studied [20].

In research related to precision cycloid reducers, scholars have fully studied needle roller bearings. Zhang et al. established a rotary needle roller bearing model of an RV reducer under mixed lubrication and analyzed the effects of contact zone roughness, output speed, ambient temperature, and lubricant on the working state of the rotary needle roller bearing [21]. Xu et al. studied the influence of cycloid modification backlash and needle roller bearing clearance on the dynamic response of an RV reducer system [22]. Lyu et al. put forward a method for the optimal design of the rotary needle roller bearing of the RV reducer, established a mathematical model of the rotary needle roller bearing, optimized the rotary needle roller bearing, and effectively improved the fatigue life of the RV reducer [23]. However, in these related studies, there is almost no research on needle roller bearing deflection.

It is worth noting that due to the processing, assembly, and complex changes in load, among other reasons, needle roller deflection and collision is inevitable. This phenomenon will aggravate the bearing damage and affect the performance of an RV reducer. RV 110E is the product model with rated torque of $110 \times 9.8 \text{ N}\cdot\text{m}$ in E series of precision cycloidal reducer. In order to further reveal the common law of bearing skew collision, taking RV 110E as an example and under the framework of multi-body dynamics theory, this paper puts forward a complete set of differential dynamics equations for roller deflection, studies the inclined collision law of rotary needle roller bearings under different loads T and different cage pocket clearances cp , and obtains the attitude angle of roller collisions. This method can calculate the deflection angle and actual contact state of the roller. Additionally, it is generally applicable to the design and calculation of aspheric roller bearings, which provides basic theoretical support for the follow-up design of aspheric roller bearings. These results also provide reference value for the practical application of, and theoretical research on, bearing life under bearing skew collisions and improving the performance of precision cycloid reducers in the future.

2. The Force Calculation of Needle Roller Bearing

In the precision cycloid reducer for robots, as shown in Figures 2 and 3, the roller-cage assembly is directly matched with the crank shaft and the cycloid wheel. The main characteristic of the roller-cage assembly is that it relates to the crank shaft to realize the eccentric swing and transmit the torque to the cycloid wheel. In this paper, when establishing the model, the inner and outer rings are used to replace the crank shaft and cycloid wheel, respectively, the inner ring of the needle roller bearing is fixed, the outer ring moves and rotates, the outer ring is loaded, and the inner ring is guided.

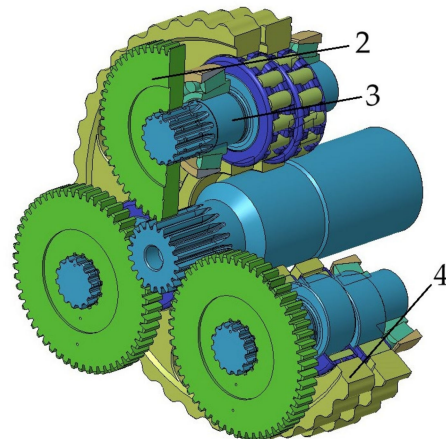


Figure 2. Model of local needle roller bearing.

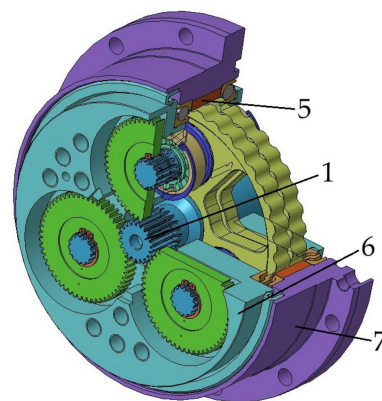


Figure 3. Structural model of RV 110E reducer.

The needle roller bearing is mainly subjected to the forces from the cycloid wheel and crank shaft, so it is necessary to analyze the cycloid wheel before calculating the forces of the needle roller bearing. The cycloid wheel is mainly subjected to the forces from the needle wheel and needle roller bearing.

The meshing force of the needle wheel is decomposed into the X direction F_X and Y direction F_Y . The meshing force of needle teeth is affected by load. Oa is the structure center of the reducer, and $O'a$ is the center of the cycloid wheel structure. e is the eccentricity. T_c is the output torque transmitted by a single cycloid wheel. Considering the uneven force of the cycloid wheel, $T_c = 0.55 \times T$. Additionally, the force of the needle roller bearing on the cycloid wheel is decomposed into F_1 , F_2 , and F_3 . F_1 is used to balance the force generated when the pin gears engage in the X direction, F_2 is used to balance the force generated when the pin gears engage in the Y direction, and F_3 is used to balance the torque generated when the pin teeth and cycloid gears engage. The force analysis of the cycloid gears is shown in Figure 4.

$$3F_3a_0 = F_x r_c \quad (1)$$

$$F_1 = \frac{1}{3} F_x \tag{2}$$

$$F_2 = \frac{1}{3} F_y \tag{3}$$

where a_0 is the radius of the distribution circle of the crank shaft and r_c is the radius of the pitch circle with clearance.

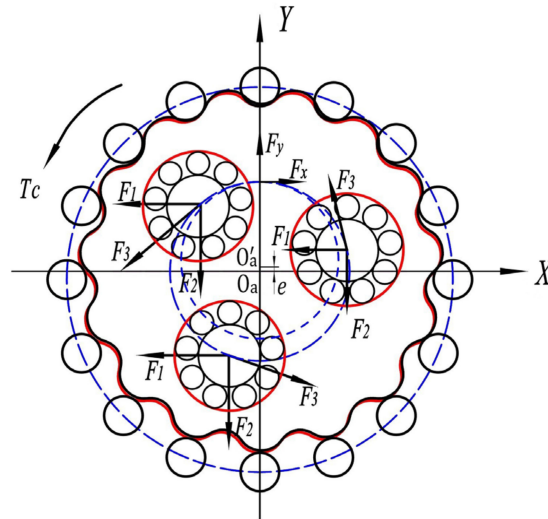


Figure 4. Force analysis model of the cycloid wheel.

The needle roller bearing bears the force from the cycloid wheel and the crank shaft. F_1' , F_2' , and F_3' are the reaction bearing of the cycloid wheel against the needle roller bearing. The force of the crank shaft is decomposed against the needle roller bearing into the radial force F_r and tangential force F_t . The force analysis diagram is shown in Figure 5. ψ is the crank shaft rotation angle. According to the law of balance, the equation of the needle roller bearing force is as follows:

$$\begin{cases} -F_r \sin \psi - F_t \cos \psi + F_3' \cos \psi + F_2' = 0 \\ F_r \cos \psi - F_t \sin \psi + F_3' \sin \psi + F_1' = 0 \end{cases} \tag{4}$$

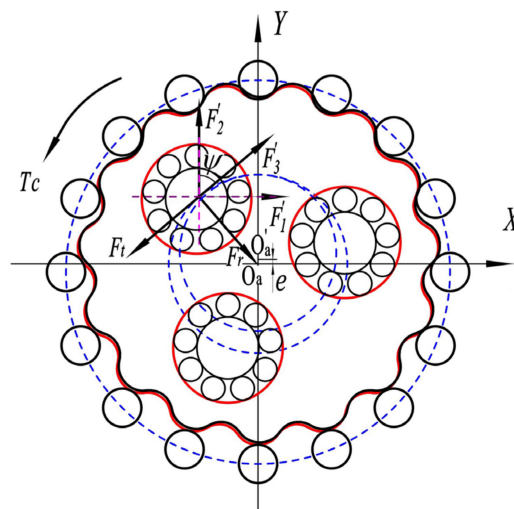


Figure 5. Force analysis of the arm bearing.

The resultant force on needle roller bearing is:

$$\begin{aligned}
 F &= \sqrt{F_r^2 + F_t^2} \\
 &= \sqrt{F_1'^2 + F_2'^2 + F_3'^2 + 2F_1' F_3' \sin \psi + 2F_2' F_3' \cos \psi}
 \end{aligned}
 \tag{5}$$

Different cage pocket clearance will affect the force between a single roller and the cage. However, different loads will affect the force of the whole needle roller bearing. For example, the force curve of the arm bearing under different loads is shown in Figure 6 when $cp = 0.2 \text{ mm}$. It is obvious that the force of the arm bearing increases with the increase in the load.

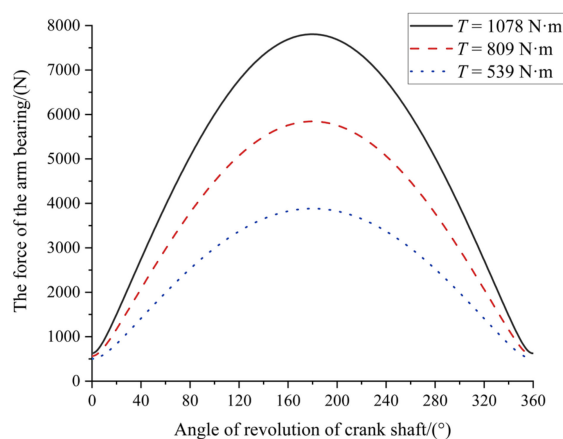


Figure 6. Force curve of the needle roller bearing.

3. The Establishment and Derivation of the Dynamic Model

3.1. The Dynamic Model of Needle Roller Bearing

In order to establish the dynamic model of needle roller bearing, this paper assumes that all the elements in the needle roller bearing are rigid bodies and that the centroid and the geometric centroid coincide and adopts the contact force algorithm of the Elastic Collision Force Model [15]. The impact contact between the cage pocket hole and the needle roller is considered the equivalent action of spring stiffness and damping. The friction force is calculated by setting a reasonable friction coefficient, and the contact between the roller and the ring is simulated using Hertz elastic contact. The dynamic model of needle roller bearing is shown in Figure 7. ω_{aj} , ω_{bj} , and ω_o are the common angular velocity, the rotational angular velocity and the cage angular velocity of the j th rolling body, respectively. ω_e is the angular velocity of the outer raceway. K_i , K_e , and K_o are the contact stiffness coefficients between the rolling body and the inner raceway, outer raceway, and cage, respectively.

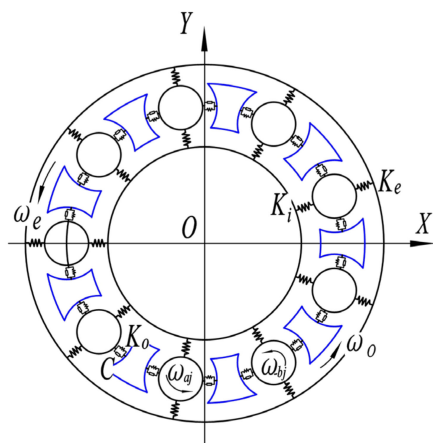


Figure 7. The dynamic model of needle roller bearing.

3.2. Defined Coordinate System

According to the structure and working conditions of needle roller bearings, the following six coordinate systems are established as shown in Figure 8:

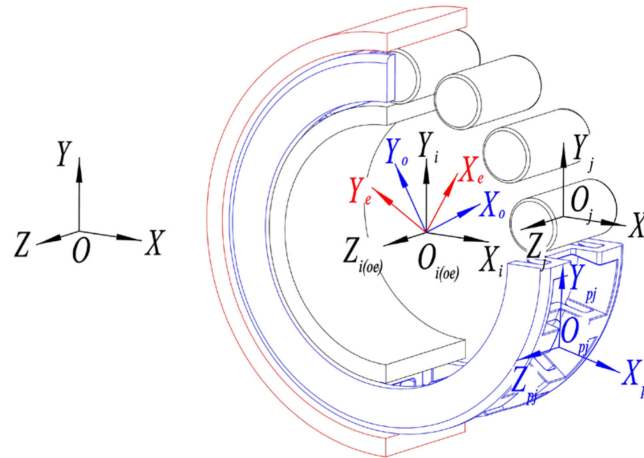


Figure 8. The coordinate system for needle roller bearing.

- (1) The fixed coordinate system $\{O\text{-}XYZ\}$ is the whole coordinate system of the precision cycloid reducer for the robot. The Z axis coincides with the rotation axis of the crank shaft, and the XY plane is parallel to the rotation plane of the whole structure. The coordinate system is unchanged in space, and other coordinate systems refer to this coordinate system.
- (2) Needle roller centroid coordinate system $\{O_j\text{-}X_jY_jZ_j\}$. Each roller corresponds to a local coordinate system, the Z axis coincides with the roller rotation axis, the XY plane is parallel to the needle roller end face, the origin coincides with the needle roller centroid, and the coordinate system rotates and moves with the needle roller, but it cannot rotate around its own Z axis.
- (3) The cage centroid coordinate system $\{O_o\text{-}X_oY_oZ_o\}$. The Z axis coincides with the rotation axis of the needle roller bearing, the XY plane is parallel to the end face of the cage, the origin coincides with the cage centroid, and the coordinate system moves and rotates with the cage.
- (4) The inner ring centroid coordinate system $\{O_i\text{-}X_iY_iZ_i\}$. The Z axis coincides with the needle roller bearing rotation axis, the XY plane is parallel to the end face of the inner ring, the origin coincides with the inner ring centroid, and the coordinate system and the inner ring fixed.
- (5) The coordinate system of the centroid of the outer ring $\{O_e\text{-}X_eY_eZ_e\}$. The Z axis coincides with the rotation axis of the needle roller bearing, the XY plane is parallel to the end face of the outer ring, the origin coincides with the centroid of the outer ring, and the coordinate system moves and rotates with the outer ring.
- (6) The central coordinate system of cage pocket hole $\{O_{pj}\text{-}X_{pj}Y_{pj}Z_{pj}\}$. At first, the coordinate system coincides with the needle roller centroid coordinate system, and then as the cage moves and rotates, the origin O_p of the coordinate system coincides with the geometric center of the cage pocket hole, and each pocket hole corresponds to its own local coordinate system.

3.3. The Nonlinear Dynamic Equations of Needle Roller

For the needle roller, in the running process, the inner ring, outer ring, and cage all have a relative effect on the needle roller, and the force and torque are shown in Figure 9.

N_{rij} and N_{rej} are the normal contact force between the inner raceway, outer raceway, and needle roller, respectively; F_{fij} and F_{fej} are the friction force between the inner raceway, outer raceway, and needle roller, respectively; M_{rij} and M_{rej} are the additional torque caused

by the contact between the inner raceway, outer raceway, and needle roller, respectively; M_{fij} and M_{fej} are the additional torque caused by the friction between the inner raceway, outer raceway, and needle roller, respectively. N_{roj} and F_{foj} are the normal contact force and tangential friction force between the cage crossbeam and the needle roller, respectively; M_{roj} is the additional moment caused by the contact between the needle roller and the cage crossbeam; N_{rijk} and N_{rejk} are the contact force between the inner raceway, the outer raceway, and the k th slice, respectively; F_{rijk} and F_{rejk} are the drag force between the inner raceway, the outer raceway, and the k th slice, respectively. N_{roj} and F_{fojk} are the normal contact force and tangential friction force between the cage crossbeam and the k th slice, respectively. In the fixed coordinate system, the nonlinear dynamic differential equations of needle roller are established, which can be expressed as follows:

$$\begin{cases} m\ddot{x}_j = (N_{rij} - N_{rej}) \sin \phi_j + (F_{fij} - F_{fej}) \cos \phi_j - N_{roj} \sin \phi_j - F_{foj} \cos \phi_j \\ m\ddot{y}_j = (N_{rej} - N_{rij}) \cos \phi_j + (F_{fej} - F_{fij}) \sin \phi_j + N_{roj} \cos \phi_j - F_{foj} \sin \phi_j \\ J_x \dot{\omega}_x = M_{fij} \cos \phi_j + M_{fej} \cos \phi_j - M_{rij} \cos \phi_j - M_{rej} \cos \phi_j + M_{roj} \sin \phi_j \\ J_y \dot{\omega}_y = M_{fij} \sin \phi_j + M_{fej} \sin \phi_j - M_{rij} \sin \phi_j - M_{rej} \sin \phi_j + M_{roj} \cos \phi_j \\ J_z \dot{\omega}_z = F_{fij} \frac{D_\omega}{2} + F_{fej} \frac{D_\omega}{2} - N_{roj} \frac{D_\omega}{2}. \end{cases} \quad (6)$$

In the formula, m is the mass of the needle roller; D_ω is the diameter of the needle roller; ϕ_j is the azimuth angle of the j th needle roller, \ddot{y}_j , \ddot{z}_j is the acceleration of the centroid displacement of the j th needle roller in the fixed coordinate system; J_x , J_y , and J_z are all the moment of inertia in the three directions of the needle roller, respectively; and $\dot{\omega}_x$, $\dot{\omega}_y$, and $\dot{\omega}_z$ all are the angular acceleration of the needle roller.

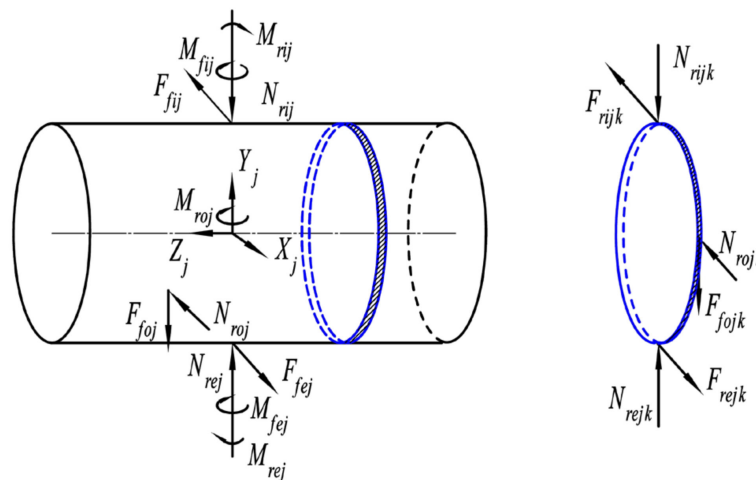


Figure 9. Force model of needle roller.

3.4. The Nonlinear Dynamic Differential Equations of Cage

The force acting on the cage is shown in Figure 10. During operation, the cage of the needle roller bearing is mainly subjected to the impact force of the needle roller.

In the figure, $\{O-XY\}$ is the reference coordinate system of the cage, e is the relative offset of the center of the cage, and Δ_{x0} and Δ_{y0} are the components of e on the X and Y axes, respectively. $e = \sqrt{\Delta_{x0}^2 + \Delta_{y0}^2}$. θ_0 is the deflection angle between the acting force of the inner and outer ring and the overall coordinate system of the cage. T_1 is the blocking moment of the cylindrical surface of the cage. T_2 is the blocking moment of the side of the cage. F_{oj} is the collision force of the rolling body in contact with the pocket hole of the cage. F_{foj} is the friction force of the rolling body in contact with the pocket hole of the cage.

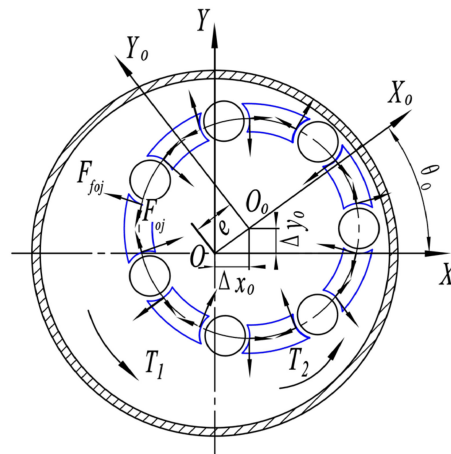


Figure 10. Force model of the cage.

The nonlinear dynamic differential equations of the cage are as follows:

$$\left\{ \begin{aligned} m_o \ddot{x}_o &= \sum_{j=1}^N (F_{oj} \cos \phi_j - F_{foj} \sin \phi_j) \\ m_o \ddot{y}_o &= \sum_{j=1}^N (-F_{oj} \sin \phi_j - F_{foj} \cos \phi_j) \\ J_{ox} \ddot{\omega}_{ox} &= \sum_{j=1}^N (M_{oj} \sin \phi_j) \\ J_{oy} \ddot{\omega}_{oy} &= \sum_{j=1}^N (M_{oj} \cos \phi_j) \\ J_{oz} \ddot{\omega}_{oz} &= \sum_{j=1}^N (F_{oj} \frac{d_m}{2}) + T_1 + T_2 \end{aligned} \right. \quad (7)$$

In the formula, m_o is the mass of the cage, N is the number of needle rollers, and \ddot{y}_o and \ddot{z}_o are the acceleration of the center of mass of the cage in the fixed coordinate system. J_{ox} , J_{oy} , and J_{oz} are the moment of inertia of the cage in the fixed coordinate system. $\dot{\omega}_{ox}$, $\dot{\omega}_{oy}$, and $\dot{\omega}_{oz}$ are the angular acceleration of the cage in the fixed coordinate system. M_{oj} is the moment caused by the contact force between the j th needle roller and the cage. d_m is the radius of bearing pitch circle.

3.5. The Nonlinear Dynamic Differential Equations of the Outer Ring

In the fixed coordinate system, when the outer ring of a bearing is subjected to periodically varying loads, the nonlinear dynamic differential equations can be expressed as:

$$\left\{ \begin{aligned} m_e \ddot{x}_e &= \sum_{j=1}^N (-N_{ej} \sin \phi_j + F_{fej} \cos \phi_j) - F \sin \omega t \\ m_e \ddot{y}_e &= \sum_{j=1}^N (-N_{ej} \cos \phi_j - F_{fej} \sin \phi_j) + F \cos \omega t \\ J_{ex} \ddot{\omega}_{ex} &= \sum_{j=1}^N (M_{ej} \cos \phi_j) \\ J_{ey} \ddot{\omega}_{ey} &= \sum_{j=1}^N (-M_{ej} \sin \phi_j) \\ J_{ez} \ddot{\omega}_{ez} &= \sum_{j=1}^N (-F_{fej}) \frac{(D_\omega + d_m)}{2} \end{aligned} \right. \quad (8)$$

In the formula, m_e is the mass of the outer ring; F is the bearing load; and \ddot{y}_e and \ddot{z}_e are the acceleration of the center of mass of Y and Z of the outer ring in a fixed coordinate

system, respectively. J_{ex} , J_{ey} , and J_{ez} are the moment of inertia of the outer ring in the fixed coordinate system. $\dot{\omega}_{ex}$, $\dot{\omega}_{ey}$, and $\dot{\omega}_{ez}$ are the angular acceleration of the outer ring in the fixed coordinate system. N_{ej} is the contact force between the j th needle roller and the outer raceway. M_{ej} is the moment caused by the contact force between the j th needle roller and the outer raceway.

4. The Dynamic Simulation and Results Analysis of Needle Roller Bearing

The design parameters of the needle roller bearings are shown in Table 1. The different loads of needle roller bearing are realized by setting different torque levels to the output flange, and the output torque was set to $T = 539 \text{ N}\cdot\text{m}$, $T = 809 \text{ N}\cdot\text{m}$, and $T = 1078 \text{ N}\cdot\text{m}$, and the cage pocket clearance was set to $cp = 0.2 \text{ mm}$, $cp = 0.3 \text{ mm}$, and $cp = 0.4 \text{ mm}$, respectively.

Table 1. Characteristic parameters of roller bearings.

Symbol	Implication	Value
Number of rollers	Z	14
Roller diameter	D	6 mm
Roller length	l	11.8 mm
Bearing bore	D_i	30 mm
Diameter of bearing pitch circle	D_m	36 mm
Bearing outside diameter	D_o	42 mm

4.1. The Collision Resultant Force of the Cage

The force vector of each roller on the cage is added together to get the resultant force of the collision between the rollers on the cage, as is shown in Figure 11. In order to facilitate the numerical view, the maximum collision force sold by the cage is shown in Table 2.

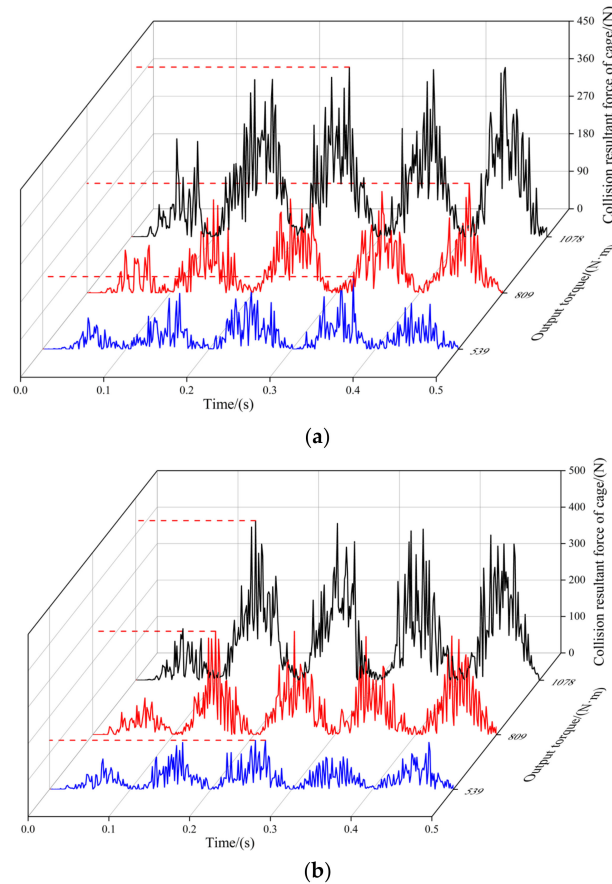


Figure 11. Cont.

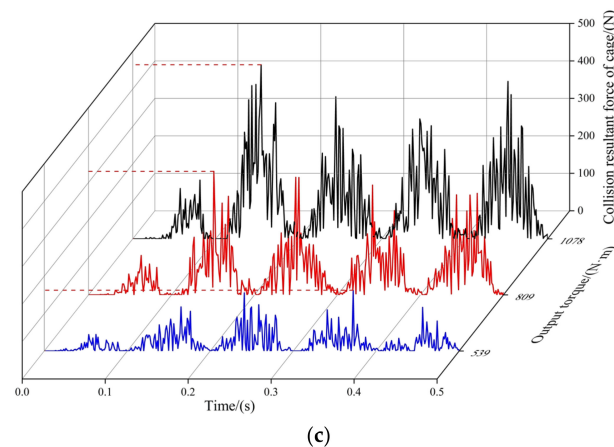


Figure 11. The resultant force of the collision between the roller and the cage under different working conditions. (a) $cp = 0.2$ mm. (b) $cp = 0.3$ mm. (c) $cp = 0.4$ mm.

Table 2. The maximum collision force of the cage.

Pocket Clearance of Cage	Output Torque	Maximum Collision Force
$cp = 0.2$ mm	539 N·m	173.93 N
	809 N·m	263.13 N
	1078 N·m	407.15 N
$cp = 0.3$ mm	539 N·m	134.58 N
	809 N·m	283.87 N
	1078 N·m	437.81 N
$cp = 0.4$ mm	539 N·m	162.09 N
	809 N·m	329.85 N
	1078 N·m	464.53 N

The resultant force on the cage is periodic. With an increase in the output torque, the collision force of the cage increases, and the fluctuation of the collision force of the cage increases.

When $T = 1078$ N·m or $T = 539$ N·m, the choice of 0.2 mm for the pocket hole gap of the cage is more stable, and when the output torque is 809 N·m, the impact force of the roller with a pocket gap of 0.3 mm is smaller.

4.2. Collision Force between a Single Roller and the Cage

In certain three time period, the force of all rollers on the cage is shown in Figure 12. The circumference represents the distribution of the rollers, and the load-bearing area can be found to change over time, but there are at least six rollers in the load-bearing area. With an increase in the output torque, the number of loaded rollers in the load-bearing zone increases. With an increase in the pocket clearance, the impact force of the cage increases markedly. In the bearing area, the amplitude of the collision force on the cage by the roller increases and decreases from small to large, which is consistent with the period of the collision force on the cage during the whole period. By observing the force on the cage at a single moment, it is found that the roller force on the middle part of the bearing area is smaller, and the roller force on both sides is larger, which shows a symmetrical trend. The tilting of the roller is restrained and the collision force between the roller and the cage is reduced. When the external load on the bearing is constant, the collision force of the cage increases with an increase in the pocket clearance. Therefore, the cage pocket clearance and the output torque have a significant impact on the cage collision force.

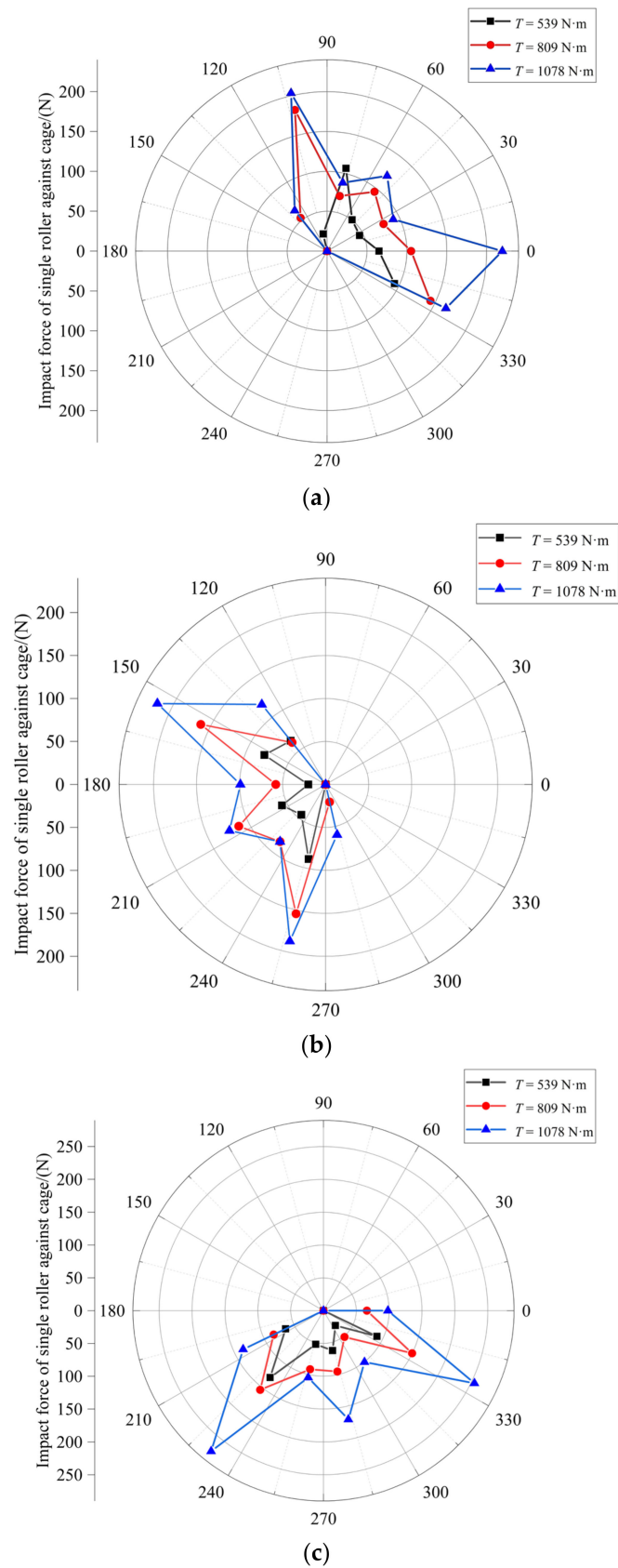


Figure 12. Impact force of roller on cage at a single moment. (a) $c_p = 0.2 \text{ mm}$. (b) $c_p = 0.3 \text{ mm}$. (c) $c_p = 0.4 \text{ mm}$.

4.3. The Change in Position and Attitude of the Roller

Deflection is a relative concept, and the roller axis and the crank axis are of the degree of non-parallelism error known as deflection. Deflection is divided into skew and askew. When roller skewing and cage collision occurs, the roller will jump up after the impact force. The collision caused by such a jump is defined as askew [24].

First, we need to define the normal plane and the cross-section plane to accurately describe the deflection and skew of the roller, the cage axis, and the roller axis through the plane defined as the normal surface of the roller. We define the surface perpendicular to the normal surface and passing through the roller axis as the tangent surface of the roller, as shown in Figure 13. Then, the angle θ between the roller axis and the normal plane is the skewing angle of the roller, as shown in Figure 14. The angle φ between the roller axis and the tangent plane is the askewing angle of the roller, as shown in Figure 15.

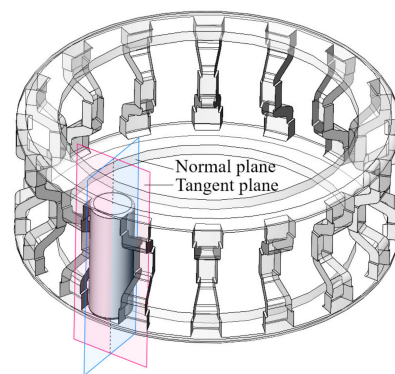


Figure 13. Schematic of the normal and tangent plane.

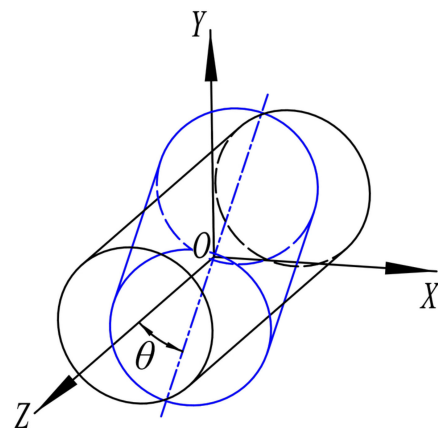


Figure 14. Schematic of the skewing angle.

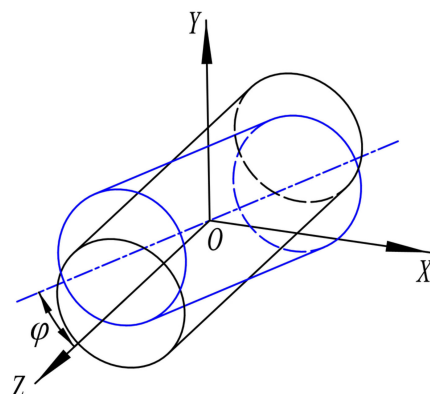


Figure 15. Schematic of the askewing angle.

In combination with the three figures, the OXY plane is the tangent plane, the OYZ plane is the normal plane, and the skewing angle and the askewing angle are the attitude angle of the roller. We assume that the angle of inclination is positive anticlockwise and negative clockwise.

Any rigid body can be accurately expressed by position and posture in the space coordinate system. The attitude of a rigid body can be represented by a 3×3 matrix, and the position of a rigid body can be represented by a 3×1 matrix. Euler angles are the only three independent angular variables that can determine the attitude of a rigid body. Therefore, the attitude of a rigid body in a coordinate system is described by three angles. There are many combinations in Euler angles; in this paper, the rotation order of Euler angles of Z - X - Z is adopted.

The rigid body rotates around the Z axis first, and the matrix is:

$$\mathbf{R}_3(Z, \alpha) = \begin{bmatrix} \cos \alpha & -\sin \alpha & 0 \\ \sin \alpha & \cos \alpha & 0 \\ 0 & 0 & 1 \end{bmatrix} \quad (9)$$

Additionally, it then rotates around the X axis, and the matrix is:

$$\mathbf{R}_1(X, \beta) = \begin{bmatrix} 1 & 0 & 0 \\ 0 & \cos \beta & -\sin \beta \\ 0 & \sin \beta & \cos \beta \end{bmatrix} \quad (10)$$

Finally, it rotates around the Z axis, and the matrix is:

$$\mathbf{R}_3(Z, \gamma) = \begin{bmatrix} \cos \gamma & -\sin \gamma & 0 \\ \sin \gamma & \cos \gamma & 0 \\ 0 & 0 & 1 \end{bmatrix} \quad (11)$$

According to the Z - X - Z rotation order, the rotation matrix of the rigid body attitude is as follows:

$$\mathbf{R} = \mathbf{R}_3(\alpha) \cdot \mathbf{R}_1(\beta) \cdot \mathbf{R}_3(\gamma) \quad (12)$$

The matrix for the position of the rigid body is:

$$\mathbf{P} = [X \quad Y \quad Z]^T \quad (13)$$

The position and pose of the rollers can then be represented by a homogeneous matrix, as follows:

$$\mathbf{Q} = \begin{bmatrix} \mathbf{R}_{3 \times 3} & \mathbf{P}_{3 \times 1} \\ \mathbf{0}_{1 \times 3} & \mathbf{1}_{1 \times 1} \end{bmatrix} \quad (14)$$

From the program, we can directly obtain the rotation angle of a single roller in the Z - X - Z order and the displacement of a single roller in relative northeast down XYZ at each moment. According to Euler angle matrix transformation, each roller corresponds to a rotation matrix at each moment. Additionally, the rotation angle data of each roller is extracted, and the pose of each roller at each moment can be obtained by collating the transformation; that is, the single roller tilt angle and skew angle.

The transformation is as follows: Let the coordinates of the roller center be \mathbf{G} , the coordinates of the cage center be \mathbf{B} , and the normal vector of the section be the unit vector of the line connecting the center of the roller relative to the northeast down center and the center of the cage relative to the northeast down, expressed as:

$$\mathbf{Q}_f = \mathbf{G} - \mathbf{B} = [X_1 - X_2 \quad Y_1 - Y_2 \quad Z_1 - Z_2] \quad (15)$$

The normal vector of the normal plane is obtained by rotating the normal vector of the tangent plane by 90° :

$$\mathbf{F}_f = \boldsymbol{\theta}_f \cdot \mathbf{Y}_z \quad (16)$$

where \mathbf{Y}_z is the rotation matrix after the normal vector of the tangent plane is rotated 90° around the Y axis of the northeast down.

$$\mathbf{Y}_z = \begin{bmatrix} 0 & 0 & 1 \\ 0 & 1 & 0 \\ -1 & 0 & 0 \end{bmatrix}$$

At each moment, the angle between the projection of the roller axis on the normal plane and the original roller axis is at an oblique angle, expressed as:

$$\varphi = \arccos\langle \mathbf{Y}, \mathbf{Y}_{tf} \rangle = \arcsin \frac{\mathbf{Y} \cdot \mathbf{Y}_{tf}}{|\mathbf{Y}| \cdot |\mathbf{Y}_{tf}|} \quad (17)$$

where \mathbf{Y}_{tf} is the projection vector of \mathbf{Y}_t on the normal plane. At each moment, the angle between the projection of the Y axis of the roller on the tangent plane and the axis of the original roller is inclined. This is expressed as:

$$\theta = \arccos\langle \mathbf{Y}, \mathbf{Y}_{tq} \rangle = \arcsin \frac{\mathbf{Y} \cdot \mathbf{Y}_{tq}}{|\mathbf{Y}| \cdot |\mathbf{Y}_{tq}|} \quad (18)$$

where \mathbf{Y}_{tq} is the projection vector of \mathbf{Y}_t on the tangent plane.

Through this method, the program calculation can obtain each roller in the unit time inclination angle and the deviation angle change; from the roller movement center of mass trace, it can be found that the trajectories of the rollers are similar, and it can be inferred that the change trend of the action force between the rollers and the cage is the same and only affected by the phase difference. Therefore, the dynamic contact characteristics of a single roller can be analyzed, and the law of all rollers can be obtained.

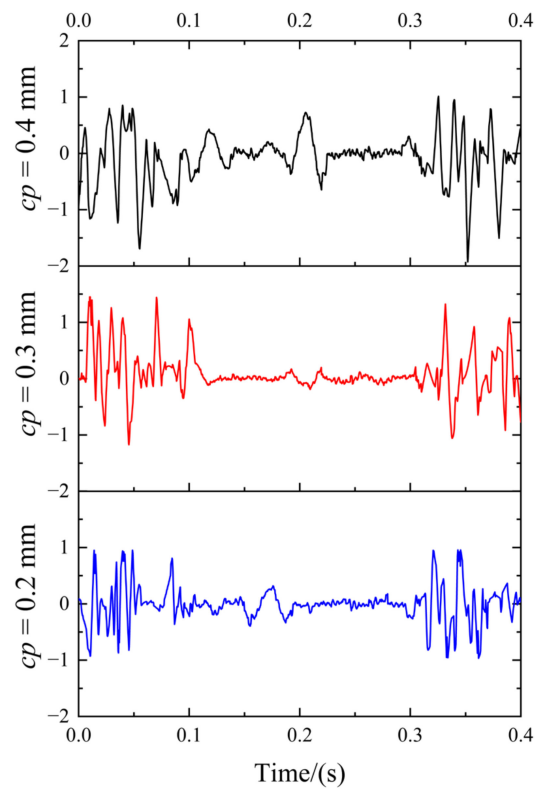
Under nine working conditions, the No. 5 roller is taken as an example and the image is used to represent the skew angle of the roller. Figure 8 shows the change curve of the tilt angle of the roller under different output torques; when the output torque is 539 N·m, the angle of the roller is changed with the output torque and the roller with a pocket clearance of 0.3 mm tilts most smoothly, and the roller with a pocket clearance of 0.2 mm fluctuates more smoothly when the output torque is increased. The variation range of the skewing angle is shown in Table 3.

Table 3. The variation range of skewing angle.

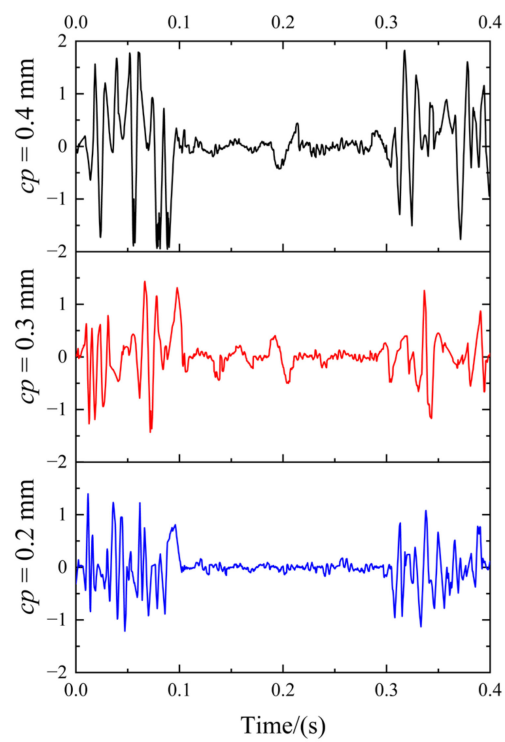
Pocket Clearance of Cage	Output Torque	Variation Range of Skewing Angle
$cp = 0.2 \text{ mm}$	539 N·m	$[-0.96^\circ, 0.95^\circ]$
	809 N·m	$[-1.21^\circ, 1.23^\circ]$
	1078 N·m	$[-1.31^\circ, 1.33^\circ]$
$cp = 0.3 \text{ mm}$	539 N·m	$[-1.17^\circ, 1.25^\circ]$
	809 N·m	$[-1.43^\circ, 1.43^\circ]$
	1078 N·m	$[-1.38^\circ, 1.36^\circ]$
$cp = 0.4 \text{ mm}$	539 N·m	$[-1.92^\circ, 1.95^\circ]$
	809 N·m	$[-1.94^\circ, 1.88^\circ]$
	1078 N·m	$[-1.91^\circ, 1.89^\circ]$

As is shown in Figure 16, when the skewing angle $\theta = 0$ and askewing angle $\varphi = 0$, the roller is the ideal state. When $\theta = 0$, the roller only has an askew angle. When $\varphi \neq 0$, the roller only has a skew angle. When $\theta \neq 0$ and $\varphi \neq 0$, the roller is in the state of skew and

askew coupling. It can be seen from the above diagram that the main state of roller motion is the coupling state of skew and askew.



(a)



(b)

Figure 16. Cont.

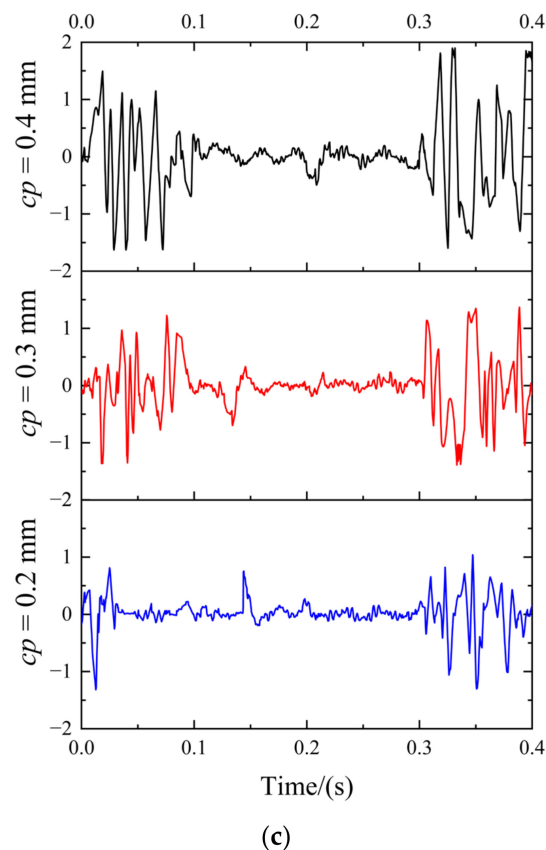


Figure 16. Variation of roller skew angle under different working conditions. (a) $T = 539$ N·m. (b) $T = 809$ N·m. (c) $T = 1078$ N·m.

4.4. The Relationship between the Roller Deflection and the Acting Force

Taking the model of $cp = 0.2$ mm, $T = 1078$ N·m as an example, the relation between the action force of the crank shaft on the roller and the inclination angle of the roller and the relation between the collision force of the cage and the inclination angle of the roller are shown in Figures 17 and 18, respectively.

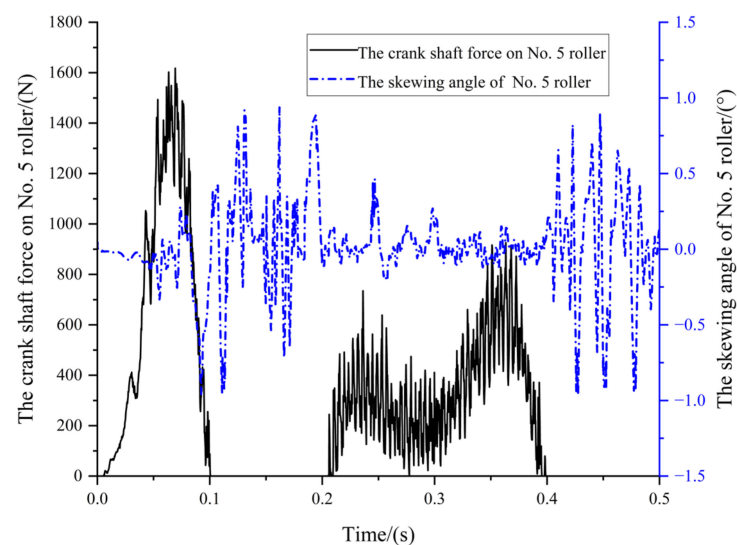


Figure 17. The crank shaft acting force on the No. 5 roller and variation of the skewing angle.

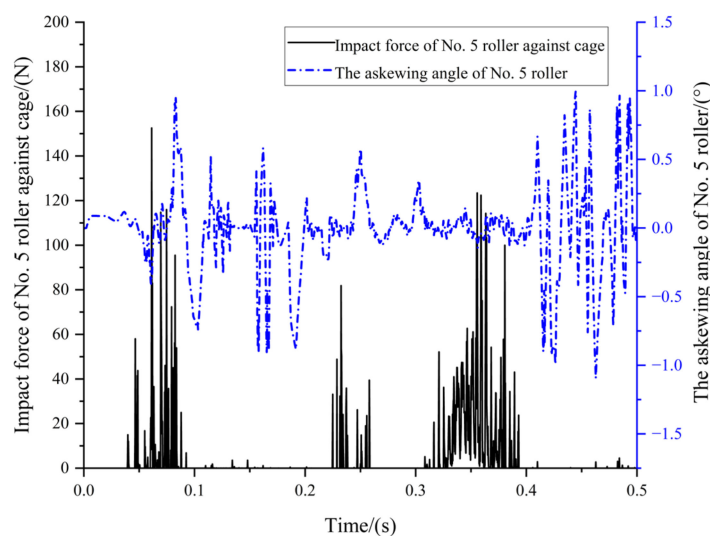


Figure 18. Collision force and the askewing angle change of No. 5 roller.

The variation trend and cause of the roller skew angle are similar to those of the skew angle. According to the simulation curve, during the period of the action force, the fluctuation of the inclination angle and the inclination angle of the roller is less, which shows that during this period, the roller enters the load-bearing area and the action of the crank shaft on the roller restrains the roller tilt and skew.

The roller can transfer part of the force to the cage only when it is acted on by the force in the bearing area. In the non-bearing area, the roller is not under the action of the force; in the free state, the skewing angle and the askewing angle fluctuate greatly.

5. Conclusions

- (1) When the roller enters the load-bearing area, the force of the crank shaft on the roller suppresses the roller's deflection. When the roller is in the non-load-bearing area, it is not affected by the force, the roller is in the free state, and the deflection phenomenon is obvious.
- (2) The cage pocket clearance affects the tilt angle of the roller. The larger the clearance, the larger the tilt angle and the larger the fluctuation range of the tilt angle. The roller's skewing and askewing show the same tendency.
- (3) The output torque affects the impact force of the rollers on the cage. The greater the output torque, the more rollers there are in the bearing area and the greater the impact force of the cage. The impact force between the roller and the cage is periodic, and this periodicity is the same as that of needle roller bearing.
- (4) When the precision cycloid reducer is used for an output torque of 1078 N·m or 809 N·m, a cage pocket clearance of 0.2 mm is the best choice. When it is used for an output torque of 539 N·m, a bearing with a 0.3 mm pocket clearance runs more smoothly.

Author Contributions: Writing—original draft preparation, Y.S.; visualization, Y.-H.Z.; funding acquisition, W.-D.H. All authors have read and agreed to the published version of the manuscript.

Funding: This research was funded by the National Key Research and Development Program of China (grant No. 2017YFB1300700) and supported by the Foundation of Liaoning Educational Committee (grant No. JDL2019017).

Data Availability Statement: Not applicable.

Conflicts of Interest: The authors declare no conflict of interest.

References

1. Boesiger, E.A.; Donley, A.D.; Loewenthal, S. An analytical and experimental investigation of ball bearing retainer instabilities. *J. Tribol.* **1992**, *114*, 530–539.
2. Creju, S.; Bercea, I.; Mitu, N. A dynamic analysis of tapered roller bearing under fully flooded conditions part 1: Theoretical formulation. *Wear* **1995**, *188*, 1–10.
3. Meeks, C.R.; Tran, L. Ball bearing dynamic analysis using computer methods: Part 1: Analysis. *J. Tribol.* **1996**, *118*, 52–58.
4. Ciavarella, E.; Decuzzi, P. The state of stress induced by the Plane frictionless cylindrical contact 1: The case of elastic similarity. *J. Solid Struct.* **2001**, *38*, 4507–4523.
5. Cui, Q.W. Discussion on needle roller skewing. *Bearings* **1980**, *1*, 4–9.
6. Pang, B.T.; Qiao, S.X.; Deng, S.E. Improving design of cage and strength analysis based on Ansys. *J. Mech. Transm.* **2010**, *34*, 76–78.
7. Cui, L.; Shi, D.F.; Zheng, J.R.; Wu, H.; Wu, F.K. Dynamic analysis of cage based on ANSYS/LS-DYNA. *J. Mech. Transm.* **2012**, *36*, 78–81+85.
8. Zhang, J.; Zhao, R.Z.; Yu, R.P. Research on dynamic characteristics of wind turbine main shaft bearing under different working conditions. *J. Mech. Strength* **2017**, *39*, 1468–1473.
9. Tu, W.B.; Liang, J.; Yang, J.W. Dynamic analysis of impact contact characteristics of the cage of a rolling bearing under variable working conditions. *J. Vib. Shock* **2022**, *41*, 278–286.
10. Gong, A.Q.; Yao, T.Q.; Xian, L.G. Dynamics Analysis on flexible cages of medium and large scale cylindrical roller bearings. *Bearings* **2019**, *02*, 6–11.
11. Liu, W.X.; Yang, X.Q.; Chen, G. Collision model and motion analysis on cage of high-speed roller bearing. *Bearing* **2003**, *9*, 1–5.
12. Wang, C.J.; Zeng, F.M.; Wang, D. Analysis on vibration characteristic of cage of mainshaft bearings in aero engine. *Bearing* **2004**, *4*, 9–11.
13. Deng, S.E.; Gu, J.F.; Cui, Y.C.; Sun, C.Y. Analysis and dynamic characteristics of cage in high-speed cylindrical roller bearing. *J. Aerosp. Power* **2014**, *29*, 207–215.
14. Yao, X. Analysis of the impact of cage in aeroengine roller bearings. Master's Thesis, Harbin Institute of Technology, Harbin, China, 2014; pp. 24–35.
15. Ma, M.M.; Liu, L.; Tian, X.Y. Profile modification for tilting coupled with skew roller in cylindrical roller bearing. *Mech. Transm.* **2017**, *41*, 68–73.
16. Zhao, Y.; Bi, M.L.; Shi, D.D. Design of high-speed cylindrical roller bearings based on control of roller skew. *Bearings* **2018**, *12*, 14–16.
17. Zhang, C.; Gu, L.; Mao, Y.Z. Modeling the frictional torque of a dry-lubricated tapered roller bearing considering the roller skewing. *Friction* **2019**, *7*, 551–563.
18. Tu, W.B.; He, H.B.; Liu, L.P. Analysis on cage dynamic characteristic of angular contact ball bearing during deceleration. *J. Mech. Transm.* **2019**, *43*, 125–129.
19. Wang, X.P.; Zhang, Y.; Ji, X.M.; Ma, S.J.; Tong, R.T. A contact-impact force model based on variable coefficient. *Vib. Shock* **2019**, *38*, 198–202.
20. Wang, Y.B.; Yang, H.S.; Xu, M.J.; Cui, Y.C.; Deng, S.E. Strength Analysis for cage of planetary wheel needle roller bearing. *J. Mech. Transm.* **2021**, *45*, 117–123+135.
21. Zhang, Z.; Wang, J.; Zhou, G.W. Analysis of mixed lubrication of RV reducer turning arm roller bearing Industrial. *Lubr. Tribol.* **2018**, *70*, 161–171.
22. Xu, L.X.; Chen, B.K.; Li, C.Y. Dynamic modeling and contact analysis of bearing-cycloid -pinwheel transmission mechanisms used in joint rotate vector reduces. *Mech. Mach. Theory* **2019**, *137*, 432–458.
23. Lyu, F.P.; Li, C.Y.; Huang, J.; Chen, B.K. Optimization design of RV reducer turning arm bearings. *China Mech. Eng.* **2020**, *31*, 1043–1048.
24. Tan, J.D. Why does the roller jump up after colliding with an obstacle. *Univ. Phys.* **1994**, *10*, 48–49.

Disclaimer/Publisher's Note: The statements, opinions and data contained in all publications are solely those of the individual author(s) and contributor(s) and not of MDPI and/or the editor(s). MDPI and/or the editor(s) disclaim responsibility for any injury to people or property resulting from any ideas, methods, instructions or products referred to in the content.